SOLID STATE SCIENCES (ISSN: 1293-2558) 39: pp. 59-68. (2015)

doi:10.1016/j.solidstatesciences.2014.11.008

EPR, Mössbauer and magnetic studies of coordination polymers of type $[Cu_xFe_y$ (dedb). $2H_2O]_n$ (dedb= dianion of 2,5-dichloro-3,6-bis (ethylamino)-1,4-benzoquinone) (x=0-1, y=0-1)

Deepshikha Singh[a], Làszlò Kòtai[b], Karoly Lazar[c] and R. L. Prasad[a*]

[a]Department of Chemistry, Faculty of Science, BHU, Varanasi-221005, India.

[b]Hugarian Academy of Sciences, Pusztaszeri u. 59-67, Budapest, Hungary, H-1025

[c] Center of Energy Research, Hungarian Academy of Sciences, Konkoly Thege M. 29-33, 1121, Budapest, Hungary.

*E-mail: rlpjc@yahoo.co.in; Tel.: +91-542-6702487; Fax: +915422368127.

Abstract

Spectroscopic studies of newly synthesized coordination polymers of the type $[Cu_xFe_y(dedb).2H_2O]_n$ {where dedb = dianion of 2,5-dichloro-3,6-bis(ethylamino)-1,4-benzoquinone (**1**); x = 1, y= 0 (**2**); 0, 1 (**3**); 0.5, 0.33 (**4**); 0.25, 0.5 (**5**); 0.125, 0.583 (**6**); 0.0625, 0.625 (**7**) and n = degree of polymerization} have been carried out by IR, Mössbauer and Electron Paramagnetic Resonance (EPR) spectroscopic techniques. Powder X-ray diffraction studies reveal the crystalline nature of the polymers. Mössbauer, EPR spectroscopic studies and Variable temperature susceptibility measurements, indicates the presence of high spin Fe (III) (S=5/2) in the polymers in-spite of using Fe(II) as starting material under inert synthetic conditions. A rare coexistence of ferromagnetism and electrical conductivity observed is discussed under present communication.

Key words: Mössbauer spectroscopy, EPR, Powder X-ray diffraction.

Introduction

In the past three decades synthesis of novel polynuclear complexes having metal ions in high spin states are central topics in the field of molecular magnetism as well as multifunctional magnetic materials [1]. Many multifunctional coordination polymers have been studied which combine optical activity [2], porosity [3], conductivity [4] and luminescence [5] with their magnetic properties. A good selection of the constituent molecules/atom could allow the appearance of an unusual combination of physical properties.

The chemistry of mixed valence multinuclear Fe (II/III) coordination polymers is of great interest because they have a significant role in solid state properties like molecular magnets either a single molecule magnet [6] or as a hybrid magnet [7-8] and as a metalloproteins [9]. Additionally multifunctional coordination polymers with π- conjugated system could provide interesting and possibly useful electronic communication between appropriate metal centers [4, 11]. An iron polymer of π- conjugated system dihydroxybenzoquinone (DHBQ) is reported to possess mixed oxidation state of metal ions [10]. Therefore, the metal-ligand networks of π- conjugated ligand in which metal ions co-exist in different oxidation states can be very interesting from conductivity as well as magnetic point of view. In this paper, we report the synthesis and characterization of iron based coordination polymers of amino-benzoquinone and their mixed metal polymers. Iron was partially substituted by copper ion to modify the magnetic and / or electronic properties in newly synthesized coordination polymers. The interesting feature is that Fe(II) is transformed into Fe(III) even when the reaction is carried out with degassed solvent and reaction under nitrogen atmosphere.

2. Experimental section

2.1. Materials and method

All the chemicals used under the present investigation were of analytical reagent grade. The Solvent used under present investigation were purified by standard procedures. 2, 3, 5, 6-Tetrachloro-1, 4-benzoquinone (chloranil) was purchased from Sigma -Aldrich and used as such without further purification for the synthesis of 2, 5-dichloro-3,6-bis(ethylamino)-1,4-benzoquinone (H_2dedb).

2.2. Synthesis of ligand (2, 5-dichloro-3,6-bis(ethylamino)-1,4-benzoquinone)

Ligand 2,5-dichloro-3, 6-bis(ethylamino)-1, 4-benzoquinone **1** (H_2dedb) was prepared by modifying literature procedure [12 - 15] as follows.

To a mixture of p-chloranil (1mmol) and anhydrous sodium acetate (7mmol) in absolute ethanol, ethylamine hydrochloride (2mmol) dissolved in absolute ethanol was added slowly drop wise with constant stirring in 30 min. The reaction mixture was further stirred for 1 hour, reflux for 4hrs. The precipitate obtained was filtered and washed with hot ethanol – water mixture many times (Yield 87%). The ligand was recrystallized from acetone.

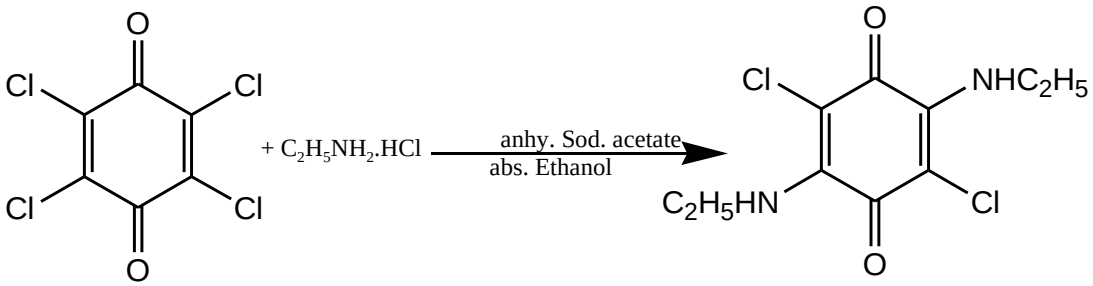

p -Chloranil 2,5-dichloro-3,6-bis (ethylamino)-1,4-benzoquinone

Anal. Calcd. for $C_{10}H_{12}O_2N_2Cl_2$ (H_2dedb): C, 45.62; H, 4.56; N, 10.64. Found (%): C, 45.54; H, 4.58; N, 10.13. ^{1}H NMR (300MHz, $CDCl_3$) (ppm): δ=7.039 (s, 2H, NH), 3.954-3.861 (q, 4H, CH_2), 1.302-1.350 (t. 6H, CH_3); ^{13}C NMR, (75 MHz, $CDCl_3$ ppm*)*: δ = 172.38 (s, 2C, C=O), 145.36 (s, 2C, C-NH), 90.92 (s, 2C, C-Cl), 39.92 (s, 2C, CH_2), 16.05(s, 2C, CH_3).

IR (KBr pellet cm^{-1}): ν (N-H) 3255, ν(C-H) 3006, 2976, 2929, 2876; ν(C=O) 1659. FAB-MS (m/z): 262, 263, 264, 265(M^+, $[M+H]^+$, $[M+2]^+$, $[M+2+H]^+$, respectively), 234 ([M-C_2H_5+H]$^+$), 176 (M- 2[NC_2H_5]$^+$).

2.2.1. Synthesis of monometallic coordination polymers of the type $[M(dedb)]_n .yH_2O$ [M = Cu **(2)**, Fe **(3)]:**

Synthesis of compound (2). $CuSO_4.5H_2O$ (2 mmol) dissolved in 15 ml distilled water was added drop wise to the solution of H_2dedb (526 mg, 2 mmol) and KOH (224 mg, 4 mmol) dissolved in 20 ml hot ethanol water mixture (1:1) with constant stirring in 30 min and stirring continued for 5 h. The reaction mixture was heated for 30 min on a water bath and allowed to stand at room temperature. The precipitate obtained was filtered and washed with hot distilled water three times. The precipitate obtained were further purified by stirring in a solvent mixture consist of 25% ethanol, 25 % acetone, 5 % DMF and 45 % distilled water for 15 min and filtered, washed with distilled water thrice followed by ethanol and dried under reduced pressure.

Compound **2**, Green solid, yield 89 %, decomposition temperature 255^{o}C, $[Cu(C_{10}H_{10}O_2N_2Cl_2).2H_2O]_n$ $(360.54)_n$: Calc. (%). C, 33.28; H, 3.88; N, 7.76; Found: C, 33.54; H, 3.91; N, 7.97.

UV-VIS (Nujol, λ_{max}, cm^{-1}): 16420, 24630, 27472, 31152, 36363, 41493.

FT-IR (cm^{-1}): ν(O-H) 3446 bs, ν(C–H) 2979, 2937, 2902, 2873w, ν_{as}(C=O) 1636 sh, ν(C=C)1529sh.

Synthesis of compound (3). To an intense reddish pink colored solution of K_2Dedb solution [50 % ethanolic solution (40 ml) of H_2dedb (0.526 g, 2 mmol) and KOH (0.224 g, 4 mmol)],

an aq. solution of $(NH_4)_2Fe(SO_4)_2 \cdot 6H_2O$ (0. 784.2 g, 2 mmol) de–aerated by passing nitrogen gas for 10 minutes before an addition was added drop wise with constant stirring over a period of ½ hr. The reaction mixture was stirred for 5 hours under nitrogen medium. The resulting reaction mixture was digested on a water bath and allowed to stand at room temperature under ambient atmosphere. The precipitate obtained was filtered and washed with hot distilled water three times. The precipitate obtained were further purified by stirring in a solvent mixture consist of 25% ethanol, 25 % acetone, 5 % DMF and 45 % distilled water for 15 min and filtered, washed with distilled water thrice followed by ethanol and dried under reduced pressure.

Compound **3**, black solid, yield 75%, decomposition temperature 224^oC, $[Fe_2(C_{10}H_{10}O_2N_2Cl_2)_3.4H_2O]_n$ $(966.68)_n$: Calc (%). C, 37.24; H, 3.93; N, 8.68; Found: C, 37.12; H, 3.60; N 8.81.

UV-VIS (Nujol, λ_{max}, cm^{-1}): 16835, 24450, 26737, 29154, 31847, 38461, 39215.

FT-IR (cm^{-1}): ν(O-H) 3404 bs, ν(C–H) 2981, 2930, ν_{as}(C=O) 1649m, ν(C=C) 1566 m.

2.2.2. Synthesis of heterobimetallic coordination polymers:

Synthesis of compound (4). The heterobimetallic polymeric complex $Cu_{0.5}Fe_{0.33}(dedb).2H_2O$, was obtained by drop wise addition of aqueous metal salt solution $(NH_4)_2Fe(SO_4)_2 \cdot 6H_2O$ (0.392 g, 1mmol) and $CuSO_4.5H_2O$ (0.250 g, 1mmol) de–aerated by passing nitrogen gas for 10 min before addition to a filtered solution of K_2Dedb [50 % ethanolic solution (40 ml) of H_2dedb (0.526 g, 2mmol) and KOH (0.224 g, 4mmol)] with constant stirring over a period of ½ hr. The reaction mixture was stirred for 5 hours under nitrogen medium followed by digestion on water bath for 15 min under ambient atmosphere and allowed to stand at room temperature. Green black precipitate obtained was filtered and washed with distilled water twice and many times with hot water followed by ethanol and dried under reduced pressure.

Compound **4**, Dark Green solid, yields 75%, decomposition temperature 230^oC, $[Cu_{0.5}Fe_{0.33}(C_{10}H_{10}O_2N_2Cl_2).2H_2O]_n$ $(347.19)_n$: Calcd (%). C, 34.56; H 4.03, N, 8.06; Cu, 9.15; Fe, 5.30, Found: C, 34.41; H, 4.01; N, 8.09; Cu, 9.45; Fe 5.65.

UV-VIS (Nujol, λ_{max}, cm^{-1}): 16233, 23094, 25316, 27397, 29154, 33222, 37593, 42372.

FT-IR (cm^{-1}): ν(O-H) 3446 bs, ν(C–H) 2981, 2936, ν_{as}(C=O) 1651sh, ν(C=C) 1520 vs.

Synthesis of compound (5). $Cu_{0.25}Fe_{0.5}(dedb).2H_2O$ was obtained by drop wise addition of aqueous metal salt solution $(NH_4)_2Fe(SO_4)_2 \cdot 6H_2O$ (0.588 g, 1.5mmol) and $CuSO_4.5H_2O$ (0.125 g, 0.5mmol) de–aerated by passing nitrogen gas for 10 minute before addition to a filtered solution of K_2Dedb [50 % ethanolic solution (40 ml) of H_2dedb (0.526 g, 2mmol) and

KOH (0.224 g, 4mmol)] with constant stirring over a period of ½ hr. The rest of the procedure is same as in the case of **3**.

Compound **5** dark black solid, yields 65%, decomposition temperature 215 ^{o}C $[Cu_{0.25}Fe_{0.5}(C_{10}H_{10}O_2N_2Cl_2).2H_2O]_n$ $(340.8)_n$: Calcd (%). C, 35.21; H, 4.10; N 8.21; Cu, 4.65; Fe, 8.19, Found: C, 35.10; H, 4.08; N 8.16; Cu, 4.87; Fe, 8.50.

UV-VIS (Nujol, λ_{max}, cm^{-1}): 16313, 23474, 26041, 28653, 32051, 35211, 39370, 45045.

FT-IR (cm^{-1}): ν(O-H) 3432 bs, , ν(C–H) 2980, 2926, ν_{as}(C=O) 1651sh, ν(C=C) 1511 vs.

Synthesis of compound (6). $Cu_{0.125}Fe_{0.583}$ (dedb).$2H_2O$ was obtained by slow addition of an aqueous metal salt solution of $(NH_4)_2Fe(SO_4)_2\cdot 6H_2O$ (0.686 g, 1.75mmol) and $CuSO_4.5H_2O$ (0.0625g, 0.25mmol) de–aerated by passing nitrogen gas for 10 minutes before the addition to a filtered solution of K_2Dedb [50 % ethanolic solution (40 ml) of H_2dedb (0.526 g, 2mmol) and KOH (0.224 g, 4mmol)] with constant stirring over a period of ½ hr. The rest of the procedure is same as described for the synthesis of **3**.

Compound **6**, black solid, yield 67%, decomposition temperature 208^{o}C.

$[Cu_{0.125}Fe_{0.583}(C_{10}H_{10}O_2N_2Cl_2).2H_2O]_n$ $(337.49)_n$: Calc (%). C, 35.56; H, 4.14; N, 8.29; Cu, 2.35; Fe, 9.64, Found C, 35.48, H, 4.12; N 8.25; Cu, 2.13; Fe, 9.81.

UV-VIS (Nujol, λ_{max}, cm^{-1}): 16181, 21598, 23752, 26809, 28490, 33557, 39062, 43103.

FT-IR (cm^{-1}): ν(O-H) 3432 bs, , ν(C–H) 2979, 2930, ν_{as}(C=O) 1651sh, ν(C=C) 1519 bs.

Synthesis of compound (7). $Cu_{0.0625}Fe_{0.625}$(dedb).$2H_2O$ was obtained by the addition of an aqueous metal salt solution of $(NH_4)_2Fe(SO_4)_2\cdot 6H_2O$ (0.735 g, 1.87mmol) and $CuSO_4.5H_2O$ (0.031 g, 0.125mmol) de–aerated by passing nitrogen gas for 10 min before addition into the filtered solution of K_2Dedb [50 % ethanolic solution (40 ml) of H_2dedb (0.526 g, 2mmol) and KOH (0.224 g, 4mmol)] with constant stirring over a period of ½ hr. The rest of the procedure is same as described for the synthesis of **3**.

Compound **7**, black solid, yield 62%, decomposition temperature 195^{o}C.

$[Cu_{0.0625}Fe_{0.625}(C_{10}H_{10}O_2N_2Cl_2).2H_2O]_n$ $(335.87)_n$: Calcd (%). C, 35.72; H, 4.16; N, 8.33; Cu, 1.18; Fe, 10.39, Found: C, 35.58; H, 4.17; N, 8.12; Cu, 1.16; Fe, 10.61.

UV-VIS (Nujol, λ_{max}, cm^{-1}): 16447, 25125, 26315, 28490, 31347, 35714, 39525.

FT-IR (cm^{-1}): ν(O-H) 3427 bs, ν(C–H) 3010, 2926, ν_{as}(C=O) 1651sh, ν(C=C) 1563 sh.

2.3. Analysis and physical measurements

The C, H and N were estimated on EAI CE 440 Elemental analyzer. Melting points of the polymeric complexes were determined in open capillaries on Gallenkamp apparatus and are uncorrected. Amount of copper and iron was estimated by atomic absorption technique on

model GBC 932 AA spectrometer. IR spectra of the solid samples were recorded on VARIAN 3100 FTIR Excalibur spectrophotometer by making KBr pellet in the range 4000–400 cm^{-1}. Following experimental parameters were used for recording the IR spectra: resolution, 4 cm^{-1}; gain, 20; scan, 32. Mössbauer data of the samples were recorded on a KFKI spectrometer, with 1 GBq $^{57}Co/Rh$ source. Isomer shift data are related to metallic α-iron. Accuracy of positional parameters is ± 0.03 mm/s. Spectra were decomposed to doublets consisting of pairs from Lorentzian-Shapes lines. The quality of the fits was reasonable. Namely, the maximum of the characterizing conventional chi-square value did not exceed 1.21. Solid state EPR spectra of the powdered samples were recorded on a Varian, USA, model E-112 ESR spectrometer. Electronic absorption spectra of the ligand and metallo polymers were recorded in Nujol mulls in the wavelength region of 11111 – 50000 cm^{-1} on SHIMADZU UV – 1700 PHARMA SPEC, UV – visible spectrophotometer. The powder X-ray diffraction pattern was obtained on RIKAGU Miniflex II desktop X-ray diffractometer using Cu Kα (λ= 1.541836 Å) radiation. Thermogravimetric (TG) thermograms were recorded on Diamond DT/GA Perkin Elmer equipment. Ade Magnetics DMS-VSM vibrating sample magnetometer model EV X was used for recording of the M-H curve. Variable temperature DC magnetic susceptibility measurements of polycrystalline powdered samples were done on quantum design SQUID magnetometer model MPMS-XL, USA, in the field of 1T in the temperature range 2 – 300K. The diamagnetic corrections were applied by using Pascal's constant. Variable temperature solid state DC conductivity of the compressed pellet of powdered samples was measured on a Keithley 236 source measure unit.

3. Results and discussion

The coordination polymers under present study were characterized by elemental analysis, IR, powder XRD, thermogravimetric analysis, Mössbauer, Electron Spin Resonance spectroscopy and variable temperature magnetic susceptibility measurements. The ligand H_2dedb was synthesized by modifying the reported method [12 - 14]. Absence of additional peaks from ^{1}H and ^{13}C NMR spectra of ligand reflects that synthesized ligand is highly pure (Fig. S1-S2). Presence of molecular ion peak at m/z 261, 262, 263, 264, 265 as $[M-H]^+$, M^+, $[M+H]^+$, $[M+2]^+$, $[M+2+H]^+$, respectively, further supports the formation of ligand H_2dedb (Fig. S3). Compound **2** is insoluble in common organic solvents such as ethanol, methanol, DCM, acetone, acetonitrile, and very slightly soluble in DMF and DMSO. Compounds **3-7**

are slightly soluble in acetone and fairly in DMF and DMSO. Attempts have been made to grow single crystal of these polymers but we did not get suitable crystals for diffraction.

3.1 IR spectra

IR spectrum of synthesized ligand H_2dedb shows characteristic ν_{as}(N-H), ν(C=O) and ν(C=C) vibrational modes at 3252, 1659 and 1582 cm^{-1}, respectively, at very similar positions to its analogue 2,5-diamino-3,6-dichloro-1,4-benzoquinone [16]. IR spectra of metallopolymers do not exhibit ν_{as}(N-H) vibrational mode indicating deprotonation of N-H protons. This indicates the involvement of nitrogen donor atoms in bonding/coordination.
The ν_{as}(C = O) vibration in metal complexes are observed at lower frequency (1636 – 1651 cm^{-1}) than that of the ligand H_2dedb (1659 cm^{-1}) [13]. Lowering of ν_{as}(C = O) vibration in metallopolymers indicates involvement of quinonic oxygen in coordination. The IR spectral results suggest that the bonding of ligand to metal ions occurs through nitrogen and oxygen donor atoms (Table S1) [17]. It is worth to be mentioned that broad band due to ν(O - H) vibration ~3450 cm^{-1} is absent in the IR spectrum of ligand H_2dedb but it is observed in spectra of polymers. Appearance of ν(O - H) vibration ~3450 cm^{-1} as broad band in the IR spectra of polymers supports the presence of water in the coordination polymers.

3.2. Powder X-ray Diffraction (PXRD) spectra

The powder XRD pattern of the compounds **2**, **3**, **4**, **7** and equal mass mixture of **2** and **3** was recorded between 2θ values 10° to 70/80°. Most of the peaks are present in the 2θ range 10 to 45°. Presence of clearly distinct 11, 17, 5 and 13 peaks in the diffractogram (Fig.1) of **2**, **3**, **4** and **7** respectively, indicates their crystalline nature [18 – 21]. Monometallic polymer **2** exhibits two peaks at 2θ values 10.21, 13.00° and **3** exhibits three peaks at 10.80, 12.20, and 13.91° whereas each of the heterobimetallic polymers **4** and **7** possesses only one peak at 13.01 and 12.03°, respectively, in the 2θ range 10° to 15°. A mixture of **2** and **3** in equal mass ratio (**EM**) exhibits three peaks at ~10. 00, 13.00 and 13.90° which are almost at the same positions to those found in monometallic polymer **2** and **3** with an average of their intensities [20]. Diffractogram of **2** exhibits a shoulder (16.20°) and four peaks (18.20, 22.35, 24.04 and 24.72°) and **3** shows six peaks (17.72, 19.32, 20.64, 21.96, 23.90 and 25.04°) in the 2θ range 15 - 26°. The presence of five peaks (~16.20, 17.72, 19.30, 22.10, 24.39°) in the diffraction pattern of EM shows the existence of peaks at almost the same positions as in respective monometallic polymer and averaging of their peak intensities. Heterobimetallic polymer **4** exhibits two broad peaks (~18.30, 25.00°) whereas, **7** exhibits five peaks (16.30,

18.00, 20.70, 22.92, 24.68°) in this 2θ range. (Table S2). Presence of peak at 20.70° and its absence ~ 22.10° in **7** as compared to **EM** indicates that **7** possess a new identity. Entirely different nature of peaks in PXRD of **4** as compared to that of **EM** corroborates its distinct identity. Similarly, change in number and nature (intensity and broadness) of peaks in diffractograms of **4** and **7** from that of **EM** supports the above conclusion. Monometallic coordination polymers **2** and **3** exhibit four and five clearly distinct peaks respectively, in the 2θ range 30 - 45°. Further, **4** possess two peaks (one broad ~34.20 and a sharp ~ 39.86°) and **7** exhibit one sharp peak ~34.70° along with three weak peaks ~30.30, 31.92 and 42.80° in the above region. **EM** exhibits four lines ~31.30, 33.04, 35.74 and 39.78° whose position do not match with those of heterobimetallic polymers **4**, **6** and **7** indicating that these polymers under present study are not a mixture of respective monometallic polymers in appropriate mole ratio.

3.3. Thermal analysis

Thermogravimetric curve (TG) of the coordination polymers **2**, **3**, **4** and **7** was recorded under air on Perkin Elmer thermal analyzer model Diamond TG/DTA. TG in combination with DTG curve of these polymers indicate that thermal degradation of monometallic polymers **2** and **3** takes place in three major steps and heterobimetallic polymers **4** and **7** occur in two steps. Magnitude of weight loss for the first step of degradation corresponds to the loss of two water molecules from **2**, **3**, **4** and **7** in the temperature range RT to 190 °C (Fig. 2). One distinct peak is observed in the DTG curve of **2** (117 ºC), **3** (141°C) and two peaks (first one very weak and second as medium) in **4** (78, 148°C) and **7** (87, 144 °C) (Fig. 3). Peaks above 100 °C in the DTG curve of **4** and **7** also supports either coordinated nature or trapped nature of water molecules under the polymeric network. Endothermic DTA peak in the above temperature range is in good agreement with loss of water molecules. Samples dried under vacuum absorb the water molecule on exposure to air indicating weakly hygroscopic nature of the polymers. Amount of water molecules absorbed by them have been found to be dependent upon the relative humidity present in the air.

Second major step of decomposition of **3** exhibits three DTG peaks (217, 262 and 282 °C) in the temperature range 160 –290 °C. Magnitude of weight loss corresponds to ~ 46 % due to the loss of ligand fragments. Exothermic DTA peaks are obtained at 224 and 280 °C in this temperature region (Fig. 4).

Magnitude of weight loss under the third step of thermal decomposition corresponds to ~12% in the temperature range 290 - 415 °C. DTG curve corresponding to the third step of degradation is observed as a very broad peak ~ 360 °C. The exothermic nature of DTA peak ~363°C probably arises due to absorption of oxygen to convert metal ion into its oxide [22].

Residue at 500°C (~32 %) presumably contains iron(III) oxide along with some carbonaceous material ($0.5Fe_2O_3$ + C) and magnitude of residue remains constant up to 700 °C. Almost similar degradation pattern is exhibited by **2** (Fig. 2). However, the third step of thermal degradation continues up to 600°C with a residual mass corresponding to ½ mole of CuO (~10 %) unlike that of **3** where final degradation ceases ~ 470 °C and final residue is much more (~32 %). It is worth to be mentioned that final residue ~10 % in case of **2** is obtained on a repeated TG curve. Powder X-ray diffractogram of the residue obtained from **2** (R_2) matches with that of CuO (Fig. 5) [23]. Completion of thermal degradation of heterobimetallic polymers **4** and **7** under the second step of degradation in contrast to three step degradation of monometallic polymers indicate that second and third step of degradation of heterobimetallic polymers merges into one step. Evidence of merging of two steps into one is obtained from DTG curve in **7** as follows. The position of first major DTG peaks under the second step of degradation of **7** (279 °C) is obtained at higher temperatures than those of the corresponding peak of **2** (270 °C) and **3** (263 °C) and second major peak at (318 °C) lower temperature than those of **2** (447 and 502 °C) and **3** (356 °C). Similarly, two DTG peaks of **4** become so close to each other that they merge and yield only one peak at 258 °C. The DTA peak position in **4** and **7** also confirms the above conclusion. These features of the thermal curves further support the distinct identity of **4** and **7** rather than a mixture of respective monometallic polymers. Nature of TG curve at the end of the second step of degradation is unique due to the strongly exothermic nature of this step of degradation as reported earlier [23]. The magnitude of residue at 600°C is found to be ~ 15 %, which is less than expected residue corresponding to the composition $(CuO)_{0.5}(Fe_{0.33}O_{0.5})$ and/or spinel $CuFe_2O_4$ (19.05%) probably due to loss of some residue at the second step of highly exothermic decomposition.

Powder X-ray diffraction data of the residue obtained by heating the polymer **4** with the heating rate 10°C/min to 600°C indicates the co-existence of CuO, (α-Fe_2O_3), (Fe_3O_4), and spinel (t-$CuFe_2O_4$) phases together (Table 1, Fig. 5) [24]. It is to be noted that final residue in case of **2** yields CuO ~ 600 °C whereas **3** results carbonaceous matter even up to 700 °C. Heterobimetallic polymer **7** results the residue having carbonaceous matter like **3** although slightly smaller in magnitude than that of **3**. By increasing the magnitude of copper

i.e. in **4** all the carbonaceous matter is lost at a much lower temperature (300°C) and result in the formation of oxides of metal ions. It may be concluded that mixed metal ions accelerates the thermal degradation. These results are further corroborated by the presence of single sharp DTG and DTA peaks at 258°C and 273°C, respectively.

3.4. Mössbauer Studies

The Mössbauer spectrum of the representative compounds **3**, **4** and **6** recorded at room temperature (300 K) and 77 K are shown in Fig. 6. Further, best fit values were obtained by decomposing the spectra to doublets composed from pairs of Lorentzian lines. Doublets characterizing Fe(III) or Fe(II) positions can clearly be distinguished by the technique. Best fit values were obtained by assuming two different neighborhoods for Fe(III) sites, and a small contribution from Fe(II) (< 10 %) in **3** and **6** (Table 2). It is worth to be mentioned that the contribution from Fe(II) is absent in the complex **4**. Isomer shift (δ) values for Fe(III) are in the 0.35 – 0.37 and 0.43 - 0.46 mm/s ranges in 300 and 77 K spectra, respectively. Quadrupole splitting (ΔE_Q) values fall within the 0.57 – 0.96 mm/s at 300 K and 0.63 – 1.04 mm/s at 77 K. These ranges of isomer shift and quadrupole splitting values are indicative of the existence of high spin octahedral Fe(III) in polymeric complexes [25]. Occurence of different Fe(III) centers in all the compounds can probably be attributed to presence of different adjacent metal centers ($Fe^{2+}/Fe^{3+}/Cu^{2+}$). Minor contributions (< 10 %) from Fe(II) positions are also revealed in compounds **3** and **6** as the characteristic, distinctly different δ and ΔE_Q values attest (> 1 and > 2 mm/s, respectively).

A small increase in isomer shift (δ) and quadrupole splitting (ΔE_Q) on decreasing the temperature could be attributed due to the second order Doppler Effect [10]. Thus, Mössbauer parameters of **3**, **4** and **6** indicate presence of high spin Fe (III) ion in corroboration with the results of magnetic moments corresponding to presence of five unpaired electrons. The relative intensity data shows the existence of predominantly Fe (III) site, however, **3** and **6** reflects the co-existence of small amount of Fe(II). It is worth to be mentioned that Fe(III) ion is present in **3**, **4** and **6** in spite of their synthesis under inert atmosphere. The presence of Fe(III) ions in all the polymeric complexes possibly arises due to a partial redox reaction between Fe(II) and amino-benzoquinone moiety and/or due to exposure of complexes to air during digestion. Therefore, ligand can oxidize Fe(II) into Fe(III) and itself reduces into its radical or other form.

Absence of Fe(II) signals from Mössbauer spectrum of **4** in contrast to **3** and **6** indicate incomplete oxidation of Fe(II) to Fe(III) taking place in **3** and **6** whereas, a complete

oxidation in case of **4**. These results show that by increasing the amount of Cu (II) in heterobimetallic polymer, the oxidation of Fe(II) to Fe(III) is enhanced. Thus, complete absence of Fe(II) from compound **4** supports the previous reports of electronic communication between two metal ions joint together by conjugated ligand dadb [20] a derivative of H_2dedb.

3.5. EPR

Solid state X- band EPR spectrum of **2** at room as well as liquid nitrogen temperature is almost similar to each other (Fig. 7 and 8). The $g_{\parallel}$ and $g_{\perp}$ values of **2** at room temperature were found to be 2.21 and 2.11, respectively. Appreciable difference between $g_{\parallel}$ and $g_{\perp}$ values indicates strong Jahn-Teller distortion around copper ion, i.e. axial elongation leading to the formation of almost square planar geometry around copper (II) [26]. The trend $g_{\parallel} > g_{\perp} > g_e$ for **2** indicates that the unpaired electron of copper ion resides in d_{x2-y2} orbital. The solid state EPR spectrum of **3** at RT exhibits two broad peaks corresponding to g values 4.3 and 2.12 where the former peak is relatively weak as compared to latter. However, former peak (g ~ 4.37) is more intense as compared to that of latter peak (g ~ 2.12) in the spectrum recorded at LNT. Increase in intensity of EPR signal at LNT as compared to that of RT arises due to increase of relaxation time as a consequence of reduced electron phonon coupling on lowering the temperature [27]. The reduction of peak intensity of the peak corresponding to g value ~ 2.12 as compared to that g value ~ 4.37 is probably due to its increased broadness as a result of increased spin exchange interaction between Fe^{3+} ions in **3 [**28**]**. Characteristics of the EPR spectrum of **3** is in good agreement for high spin Fe (III) (d^5) with the distorted octahedral geometry having ^6A_1g ground state [28-34].

Solid state EPR spectrum of **7** at LNT exhibit three peaks with g values 4.37, 2.26 and 2.07. The peak at g value 4.37 is very weak and broad. The position of former two g values (4.37 and 2.26) in the EPR spectrum of **7** at LNT is very close to the EPR signals of **3** while position of latter two peaks (2.26 and 2.07) are close to those of EPR signals corresponding to $g_{\parallel}$ and $g_{\perp}$ values of **2** [27,29-34]. Thus, second peak corresponding to g value ~ 2.26 may be considered to arise as a consequence of overlap of peaks due to Fe(III) and Cu(II) ions. These characteristics of the EPR signals indicate octahedral environment around Fe (III) ion and square planar arrangement around Cu (II) in the compound **7**. The room temperature EPR spectrum exhibit only two peaks corresponds to g values 2.26 and 2.07 at the same position as in LNT. However, the intensity of EPR signal corresponding to the g value ~ 4.3 is not observed at RT probably due to reduction of intensity by increase

electron phonon coupling [27] and/or due to increased spin exchange interaction between Cu^{2+} and Fe^{3+} at higher temperature (RT). Based on above observation, it may be concluded that on doping of Cu(II) ion in coordination polymers of Fe(III), the magnitude of electron phonon coupling and spin exchange interactions increases.

The polymer **4** exhibits two peaks with g values 2.26 and 2.11 at RT. The EPR signal at g value 2.26 of **4** is more intense as compared to the peak at g value 2.11 whereas just a reverse trend of intensity of signals is observed in case of **2**. Higher intensity of the peak at g value 2.26 than that of 2.11 arises due some contribution to this peak by signal arising from Fe(III) ion in addition to Cu(II) as in case of **7**. Further, interesting observation is that the peak at g ~ 2.26 in **4** is more intense than those of the corresponding peak of **7** and **2**. It is worth to be mentioned that the peak at g value ~ 2.26 in **4** is more intense than those of the corresponding peak of **7** and **2** indicating coexistence of both metal ions (Fe^{3+} and Cu^{2+}) in the polymer **4**. Solid state EPR spectrum of **4** at RT (Fig. 7) is almost identical to its spectrum at LNT except the intensity is low. The EPR signal arising from Fe(III) ion at g value ~ 4.37 completely disappear in the spectra of **4** even at LNT. Thus the intensity of the peak at g value ~4.37 is found in order **3**>**7**>**4**. Thus absence of EPR signal at g value ~4.37 from **4** corroborates our conclusion that on doping of Cu^{2+} ion in polymer of Fe(III), the electron phonon coupling and spin exchange interaction increases in the present compounds.

3.6. Magnetic studies

The magnetic properties, magnetization (M) versus applied field (H) curves of **2**, **3**, **4** and **7** were recorded on vibrating sample magnetometer (VSM) system with magnetic field strength -20 kOe to 20 kOe at room temperature (296 K). The M-H curve of the monometallic polymer **2** is non linear and saturation is achieved within the field strength ±3000Oe. Narrow hysteresis loop indicates it to be soft magnetic material with antiferromagnetic behavior between adjacent metal centers Fig. 9(a) and (b) [35].

The smaller magnitude of the observed magnetic moment of **2** (1.58 B.M) than the spin only value (1.73 BM) further supports the existence of antiferromagnetism. Saturation of magnetization for **3**, **4** and **7** is not achieved even upto 20 kOe indicating existence of ferro/ferrimagnetic and/or superparamagnetic interactions between different metal centers [36]. However, the curvature of **3** and **7** is very close to paramagnetic materials and significantly different from that of **4**. Magnetic moment calculated per Fe atom as $\mu_{eff} = 2.82*(\chi_m T)^{1/2}$ from the M-H curve for the compounds **2**, **3**, **4** and **7** are found to be 1.58, 7.13, 6.60 and 8.75B.M respectively (Table S3). These data indicate that **2** and **4** exhibit lower

magnetic moment than those calculated for respective spin only values indicating presence of antiferromagnetic and ferrimagnetic behavior. However, observed a magnetic moment of **3** and **7** are more than the spin only value calculated for high spin Fe (III) suggesting the existence of ferromagnetic behavior.

Variable temperature (2-300K) DC susceptibility measurement on SQUID magnetometer at the constant applied magnetic field of 10kOe for **3**, **4** and **6** is represented in Fig 10a-c. The magnetic moment values of **3**, **4** and **6** suggest that the iron is present as a high spin Fe (III) state in these coordination polymers in the temperature range 30-300K. The μ_{eff} (effective magnetic moment) vs T (temperature) plot of polymers **3**, **4** and **6** indicates ferromagnetic interaction in the high temperature region (150 -300K) and antiferromagnetic behavior at low temperature (<150 K). The magnetic moment value in **3**, increases from 300K (μ_{eff} = 7.17 BM) to a maximum at 150K (μ_{eff} = 8.0BM) followed by a decrease to a minimum at 2K (μ_{eff} = 2.96BM) (Fig. 10 a). There is a gradual decrease in magnetic moment from 150 K (μ_{eff} =8.0 B.M.) to 30K (μ_{eff} = 5.98 BM) which is close to the spin only value as expected for S=5/2. Therefore, this decrease could be due to weak interchain / intrachain interactions. Sudden drop of moment from 30 K to 2 K may be attributed due to antiferromagnetic interaction and/or zero field splitting (ZFS) [37]. Hence, magnetic properties of **3** show significant ferromagnetic as well as antiferromagnetic interactions. A similar trend is observed in the case of **6** where Fe (III) ions are doped with 17.6 mole percent of Cu (II). So, both ferromagnetic as well as antiferromagnetic interactions are operating in **3** and **6** depending upon temperature range. Magnetic moment value of **4** at room temperature (6.37B.M.) is less than that counted for a spin only value per Fe (III) atom (8.50 B.M) indicating antiferromagnetic interaction like that in case of **2**. However, magnitude of μ_{eff} gradually increases in going from RT (300 K) to 118 K up to 7.72 B.M, i.e very close to spin only value. On further lowering of temperature the μ_{eff} value starts decreasing. This indicated that there is alternate Fe(III) and Cu(II) ions are bridged by conjugated ligand Dedb, the antiferromagnetic interaction predominates above and below 118K. Thus, the coordination polymers under present study, exhibit dual magnetic behavior: ferromagnetic at higher temperature and antiferromagnetic at lower temperature.

3.7. Solid state electrical conductivity

Variable temperature solid state DC electrical conductivity of the compressed pellet of powdered polymers prepared at 6 ton pressure and cured at 120°C was measured by two probe method. Specific conductance of coordination polymer was calculated using the

equation $\sigma = t/RA$ {R= dc resistance from I-V curve, A= cross sectional area and t= pellets thickness}. Plot of electrical conductivity (log σ) versus the temperature (1000/T) for the solid state electrical conductivities of monometallic polymers **2, 3** and heterobimetallic polymers **4** – **7** are shown in Fig. 11.

The solid state electrical conductivity of all the polymers increases with increasing the temperature which indicates that they are semiconductors [20]. Room temperature electrical conductivity of monometallic iron polymer **3** is less than monometallic copper polymer **2**. However, with increase of temperature the electrical conductivity of **3** increases much more than that of **2,** and after 80^{o}C conductivity of **3** becomes more than that of **2**. Room temperature conductivity of heterobimetallic polymers **4** and **7** are higher than those of monometallic polymers **2** and **3.** However, after 80 $^{\circ}$C, the conductivity of **4** becomes less than the conductivity of **3**. Lesser conductivity exhibited by **5** and **6** than those of **2** and **3**. In going from **3** to **7** i.e on doping of 9% Cu(II) ions, the magnitude of electrical conductivity increases ~ ten times. The compound **7** shows highest conductivity among all these polymers at all the temperatures under present study. This indicates that conductivity of conjugated coordination polymers increases on substituting iron metal ion with copper metal ions. This is possible by injection of unpaired electron from copper metal ion onto the conjugated chain of ligand through π-back bond between Cu (II) and coordinated donor atoms of the ligand. On further increase of dopant concentration from 9 to 17.6% i.e in going from **7** to **6** conductivity decreases. Subsequent increase of dopant concentration from 17 to 33 % i.e in going from **6** to **5** the magnitude of conductivity further decreases to the lowest value probably due decrease in no. of charge carriers on substituting Fe(III) by Cu(II). However, on further increase of dopant concentration from 33 to 60% i.e on moving from **5** to **4** the magnitude of conductivity is found to be increased. In pure Cu(II) polymer i.e. increasing dopant concentration from 60 to 100% conductivity further decreases.

This trend shows a periodic behavior of solid state electrical conductivity with function of Fe/Cu concentration. Room temperature conductivity of these polymers are in the order **7**>**4**>**2**>**3**>**6**>**5**. Band gap calculated at room temperature using equation 2.303x8.314x0.01xSlope for coordination polymers **2**, **3**, **4**, **5**, **6** and **7** are 0.225, 0.667, 0.367, 0.489, 0.377 and 0.451eV, respectively.

Conclusion

The composition of synthesized coordination polymers was established by elemental analysis and metal estimation repeatedly showing the presence of Fe (III) in synthesized

coordination polymers in spite of using Fe(II) salt as starting material. In coordination polymers **3**, **4** and **6**, presence of high-spin ferric ion (S=5/2) in octahedral environment was confirmed by Mössbauer followed by magnetic and EPR spectroscopy. Powder X-ray diffraction studies suggest that the synthesized heterobimetallic polymers are new entities not the combination of monometallic polymers in appropriate molar ratio. Variable temperature magnetic studies clearly indicates no spin- state cross over taking place room temperature to 77 K. Mössbauer studies also suggest the presence of only traces of Fe (II) ion in coordination polymers **3** and **6**. The M-H curve of **2** and **4** shows the presence of antiferromagnetic and ferrimagnetic coupling respectively. Variable temperature magnetic moment data show the existence of strong ferromagnetic coupling in polymers **3** and **6**, whereas, in case of **4** (having 60% cupric ion) antiferromagnetism is observed. The antiferromagnetic interaction gradually decreases with decreasing temperature from RT to 118 K and again increases below this temperature. All the polymers exhibit semiconducting property and show periodic behavior of solid state electrical conductivity with function of Fe/Cu concentration.

Acknowledgement

Authors are thankful to the Head, Department of Chemistry, Faculty of science, Banaras Hindu University, for providing lab facilities. Thanks are also due to Head, Ceramic Engg. IIT, BHU for powder XRD, Dr. Prasun Kumar Roy from CFEES, DRDO, New Delhi for TG, and Dr. Manivel Raja from DMRL, DRDO, Hyderabad for providing, VSM analyses. UGC- DAE consortium for Scientific Research, Indore, is gratefully acknowledged for SQUID magnetometer. One of the authors is thankful for financial assistance from UGC and CSIR, New Delhi.

Appendix A. Supplementary materials

IR data of **1-7** and Powder XRD data of **1-4** and **7** is tabulated in Table S1 and S2 respectively. Magnetic moment data is given in Table S2. The ^{1}H, ^{13}C NMR, FAB Mass spectra of ligand H_2dedb and the EPR spectra of polymers **2**, **3**, **4**, **7** (RT and LNT) in g values are given in Fig. S1-S5, respectively.

References

[1] H. Z. Kou, S. F. Si, S. Gao, D. Z. Liao, Z, Jiang, S. P. Yan,Y. G. Fan and G.L. Wang. Eur J. Inorg. Chem. (2002) 699 -702.

[2] L. K. Thompson, S. K.Mandal, S. S. Tandon, J. N. Brisdon and M. K. Park, Inorg. Chem. 35 (1996) 3117.

[3] E. Ruiz, P. Alemany, S. Alvarez and J. Cano, J. Am. Chem. Soc. 119 (1997) 1297.

[4] S. V. Kolotilov, O. Cador, F. Pointillart, S. Golhen, Y. L. Gal, K. S. Gavrilenko , L. Ouahab* J. Mater. Chem., 20 (2010) 9505–9514.

[5] K. K. Nanda, L. K. Thompson, J. N. Bridson and K. Nag, J. Chem. Soc., Chem. Commun. (1994) 1337.

[6] A. L. Barra, A. Caneschi, A. Cornia, F. Fabrizi de Biani, D. Gatteschi, C. Sangregorio, R. Sessoli, L. Sorace, J. Am. Chem. Soc. 121 (1999) 5302-5310.

[7] C.Mathoniere C. J. Nuttall, S. G. Carling, P. Day, Inorg. Chem. 35 (1996) 1201-1206.

[8] M. Clemente-Leon, E. Coronado, M. Lopez-Jorda, Dalton Trans. 39 (2010) 4903-4910.

[9] J. Dubach, B. J. Gaffney, K. More, G. R. Eaton, S. S. Eaton, Biophysical Journal 51 (1991) 1091-1100.

[10] J. T. Wrobleski, D. B. Brown, Inorg. Chem. 18 (1979) 498-504.

[11] C. G. Cameron, P. G. Pickup, Chem. Comm., (1997) 303 – 304.

[12] K. Wallenfels, W. Draber, Justus Liebigs Annalen der Chemie 667 (1963) 55-71.

[13] K. Wallenfels, W. Draber, Tetrahedron 20 (1964) 1889-1912.

[14] R. Foster, Recueil des Travaux Chimiques des Pays-Bas 83 (1964) 711-17.

[15] K. Fickentscher, Archives of Pharmacy and reports of the German Pharmaceutical Society 302 (1969) 119-25.

[16] R. L. Prasad, A. Kushwaha, Suchita, M. Kumar and R. A. Yadav, Spectrochimica Acta Part A, 69 (2008) 304 – 311.

[17] S. I. Mostafa Transition Met.Chem., 24 (1999) 306- 310.

[18] L. V. Azaroff, M. J. Buerger, The Powder Method in X-ray Crystallography, McGraw-Hill, New York, 1958.

[19] S.A. Sallam, Trans Met. Chem. 31 (2006) 46-55.

[20] R.L. Prasad, A. Kushwaha, O.N. Srivastava, J. solid state chem. 196 (2012) 471- 481.

[21] S. Kawata, S. Kitagawa, I. Furuchi, C. Kudo, H. Kamesaki, M. Kondo, M. Katada and M. Munakata, Mol. Cryst. Liq. Cryst. 274 (1995) 179-185.

[22] S. T. Breviglieri, E.T. G. Cavalheiro1, G. O. Chierice, Thermochim. Acta 356 (2000) 79-84.

[23] R.L. Prasad, A. Kushwaha, D. Singh, Thermochim. Acta, 511 (2010) 17-26.

[24] G. F. Goya, H. R. Rechenberg, J. Z. Jiang, J. Appl. Phys. 84 (1998) 1101-1108.

[25] N.N. Greenwood, T.C. Gibb, Mössbauer Spectroscopy, Chapman & Hall, London, 1971, pp. 162, 206.

[26] B. A. Goodman, J. B. Raynor, Adv. Inorg Chem. & Radiochem. 13 (1970) 135-362.

[27] V.A. Ivanshin, M. R. Gafurov, I. N. Kurkin, S. P. Kurzin, A. Shengelaya, H. Keller, M. Gutmann, Physica C 307 (1998) 61–66.

[28] R. Berger, J. Kliava, E. Yahiaoui, J. C. Bissey, P. K. Zinsou and P. Beziade, J. Non-Cryst. Solids 180 **(**1995) 151-163.

[29] V. Luca, C. M. Cardile, Clays and Clay Minerals 37 (1989) 325-332.

[30] S. H. Anzaldo, N. S. Morales, R. Z. Ulloa, R. Escudero, M. de. R. Hoz, Y. R. Ortega, J. of Molecular Structure 1040 (2013) 39–46.

[31] M. J. Gunter, N. M. Lewis, S. M. Keith, Paul E. Clark, J. Am. Chem. Soc. 103 (1981) 6184-6787.

[32] C. T. Brewer, G. Brewer, L. May, J. Sitar, R. Wang, J. Chem. Soc. Dalton Trans. (1993) 151- 155.

[33] C. S. Jimenez, F. Shafizadeh, Current Microbiology, 10 (1984) 281- 286.

[34] Y. Bulach, D. Mandon, R. Weiss, Angew. Chem. Int. Ed. Engl. 30 (1991) 572-575.

[35] Li. Ya-Min, Xiao. Chang-Yu, Zhang. Xu-Dong, Xu. Yan-Qing, Luna. Hui-Jie and Niu. Jing-Yang, Cryst. Eng. Comm, 15 (2013) 7756-7762.

[36] N. M. Deraz, Int. J. Electrochem.Sci. 7 (2012) 4608–4616.

[37] I. Salitros, R. Boca, R. Herchel, J. Moncol, I. Nemec, M. Rub, and F. Renz, Inorg. Chem. 51 (2012) 12755−12767.

Table caption

Table 1. 2θ values of the residues of polymers **2** and **4** obtained at 600°C

Table 2. The Mössbauer spectral parameters of polymers **3**, **4** and **6.**

Figure captions

Fig.1. Powder X-ray diffractogram of polymers **2**, **3**, **4**, **7** and equimolar mixture **(EM)**.

Fig. 2. TG thermogram of **2**, **3**, **4** and **7**.

Fig. 3. DTG thermogram of **2**, **3**, **4** and **7**.

Fig. 4. DTA thermogram of **2**, **3**, **4** and **7**.

Fig. 5. PXRD of residue of **2** and **4** obtained at 600°C.

Fig. 6. The Mössbauer spectrum of **3**, **4** and **6** at 300 and 77K.

Fig.7. Solid state EPR spectra of **2**, **3**, **4** and **7** at RT.

Fig. 8. Solid state EPR spectra at **2**, **3**, **4** and **7** at LNT.

Fig. 9 (a). M-H curve of **2**, **3**, **4** and **7 (b)** in low field region.

Fig.10 (a-c). Temperature dependence of μ_{eff} and χ_m^{-1} **(a)** for **3**, **(b) 4** and **(c) 6.**

Fig. 11. Variable temperature solid state electrical conductivity of the polymers **2-7**. The inset image shows variation of conductivity as a function of dopant concentration at 50°C.

Table 1. 2θ values for the residues of **2** and **4** obtained at 600°C.

Residue of polymer **2** (degree)	Residue of polymer **4** (degree)
32.46	32.42 (CuO)
35.46	33.18 (α-Fe_2O_3)
38.66	**35.64** (CuO), (α-Fe_2O_3), (t-$CuFe_2O_4$)
48.68	37.06 (Fe_3O_4), (t-$CuFe_2O_4$)
53.54	**38.86** (CuO)
58.28	41.04 (α-Fe_2O_3) , (t-$CuFe_2O_4$)
61.48	49.58 (CuO), (α-Fe_2O_3) (broad peak)
65.70	53.86 (α-Fe_2O_3), (t-$CuFe_2O_4$) (broad peak)
66.20	57.70 (CuO), (α-Fe_2O_3), (t-$CuFe_2O_4$) (broad peak)
68.04	62.52 (α-Fe_2O_3), (t-$CuFe_2O_4$)

Highest intensity peaks are marked as bold

Table 2. The Mössbauer spectral parameters of **3**, **4** and **6**.

Temperature		**300** K				**77** K			
Compound	**Ion**	**δ**	**ΔE_Q**	**FWHM**	**RI**	**δ**	**ΔE_Q**	**FWHM**	**RI**
3	Fe^{3+}	0.37	0.57	0.40	53	0.46	0.60	0.53	54
	Fe^{3+}	0.37	0.96	0.50	43	0.46	1.04	0.53	38
	Fe^{2+}	1.01	2.28	0.48	3	1.33	2.14	0.68	8
4	Fe^{3+}	0.35	0.56	0.36	59	0.46	0.59	0.44	69
	Fe^{3+}	0.35	0.96	0.38	41	0.46	1.06	0.39	31
6	Fe^{3+}	0.35	0.60	0.35	51	0.44	0.63	0.41	58
	Fe^{3+}	0.36	0.96	0.41	42	0.43	1.10	0.41	33
	Fe^{2+}	1.29	2.25	0.27	6	1.52	2.45	0.39	9

δ: isomer shift, relative to α-iron, mm/s; **ΔE_Q**: quadrupole splitting, mm/s; FWHM: full line width at half maximum, mm/s; RI: relative intensity, %. The accuracy of the positional parameters is ca. ± 0.03 mm/s.

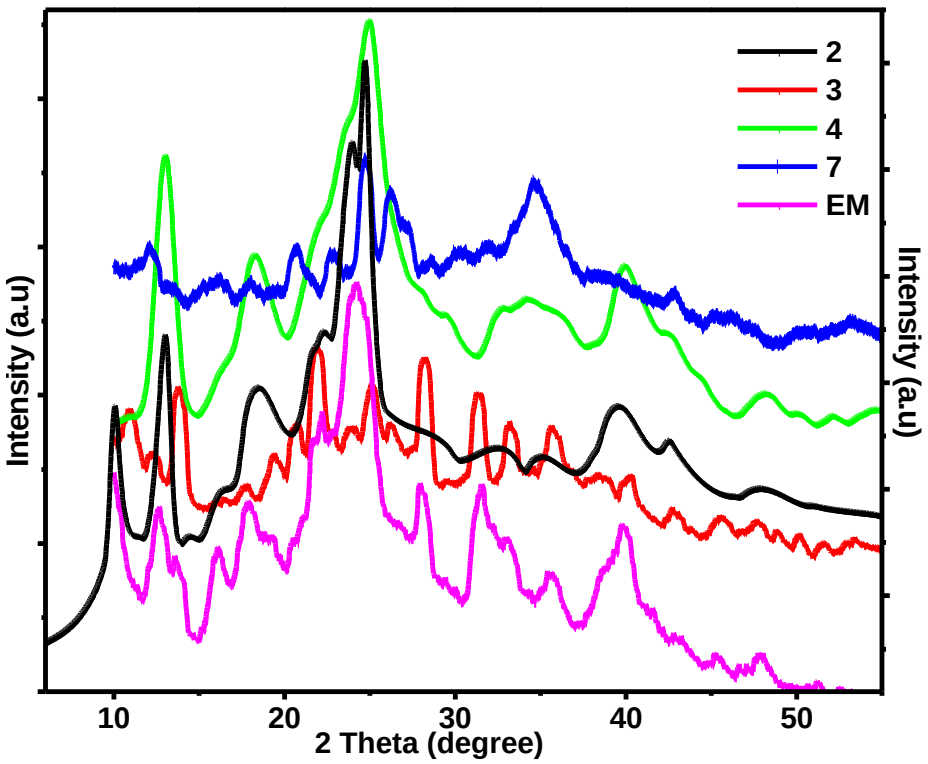

Fig. 1. Powder X-ray diffractogram of polymers **2**, **3**, **4**, **7** and equimolar mixture **(EM)**.

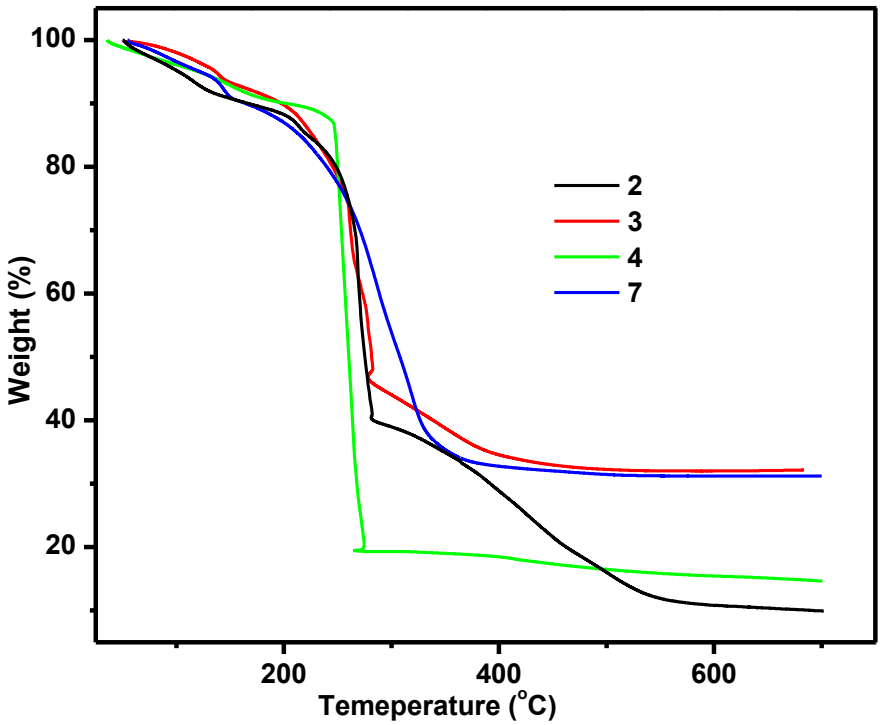

Fig. 2. TG thermogram of **2**, **3**, **4** and **7**.

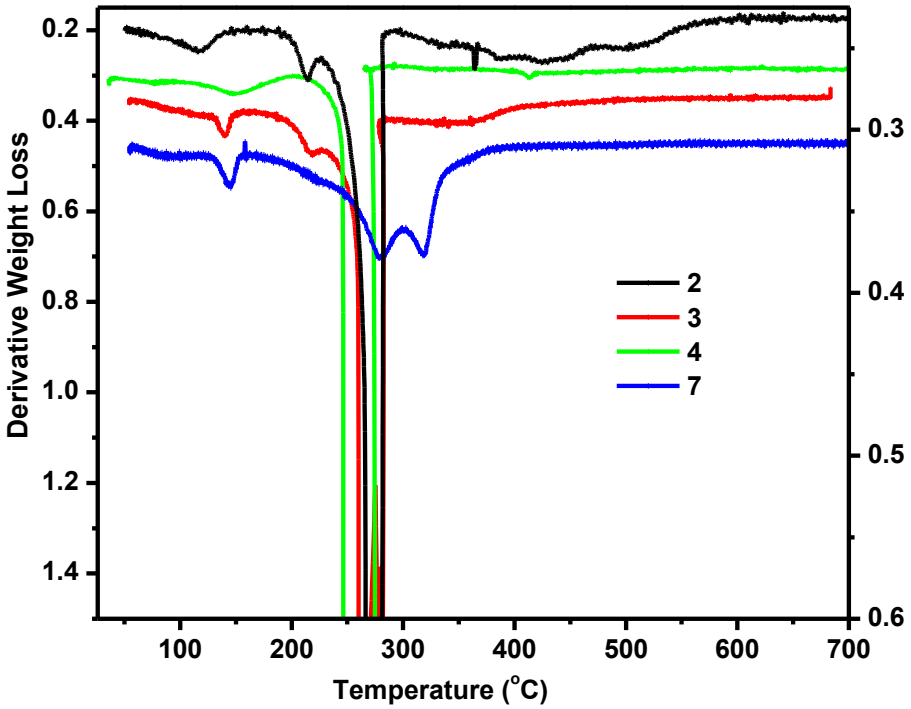

Fig.3. DTG thermogram of **2**, **3**, **4** and **7**.

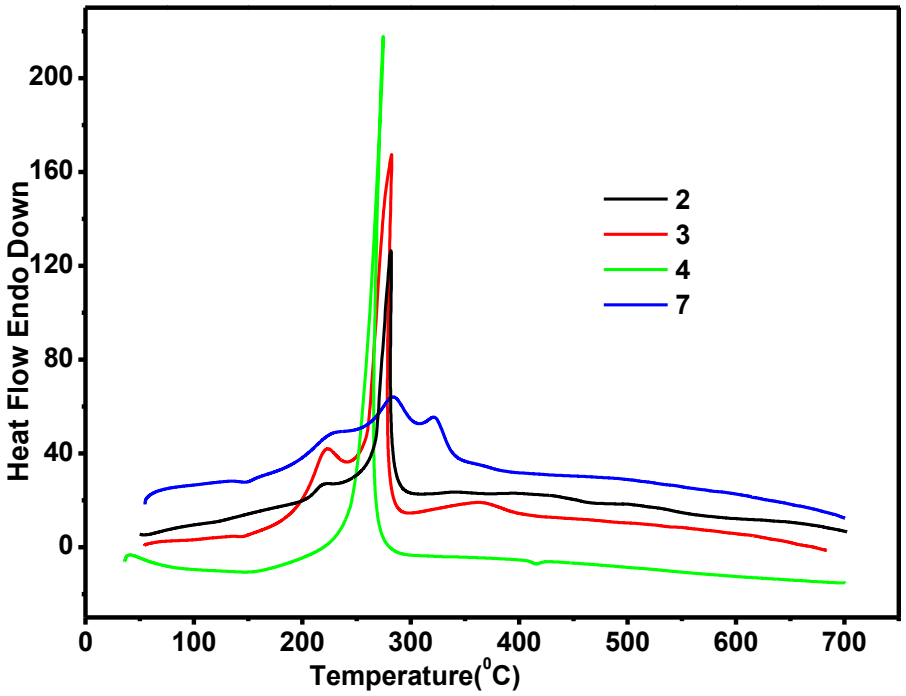

Fig. 4. DTA thermogram of **2**, **3**, **4** and **7**.

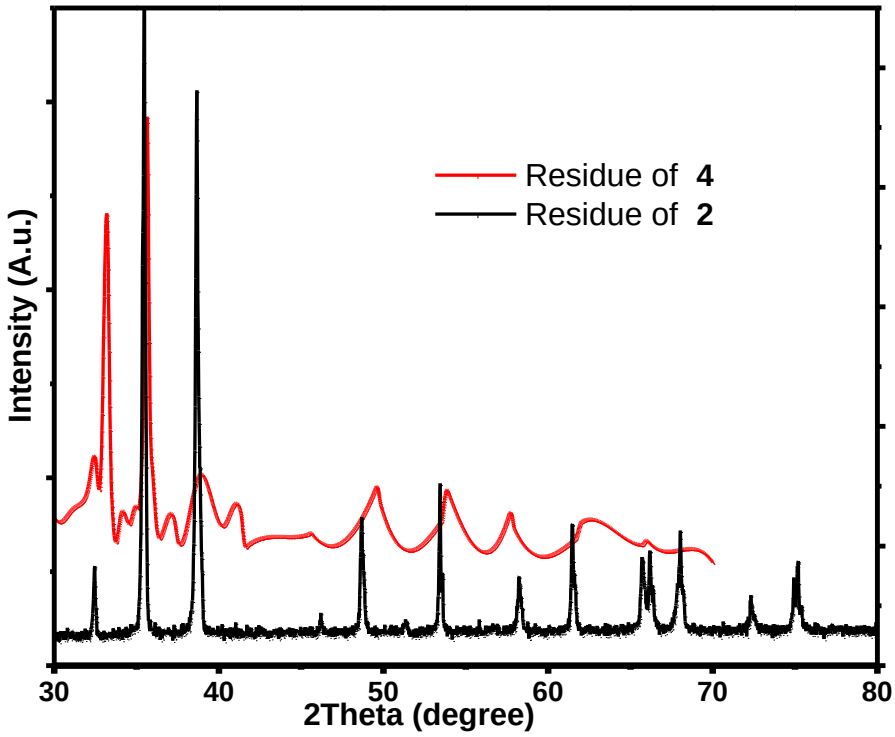

Fig. 5. PXRD of residue of polymers **2** and **4** obtained at 600°C.

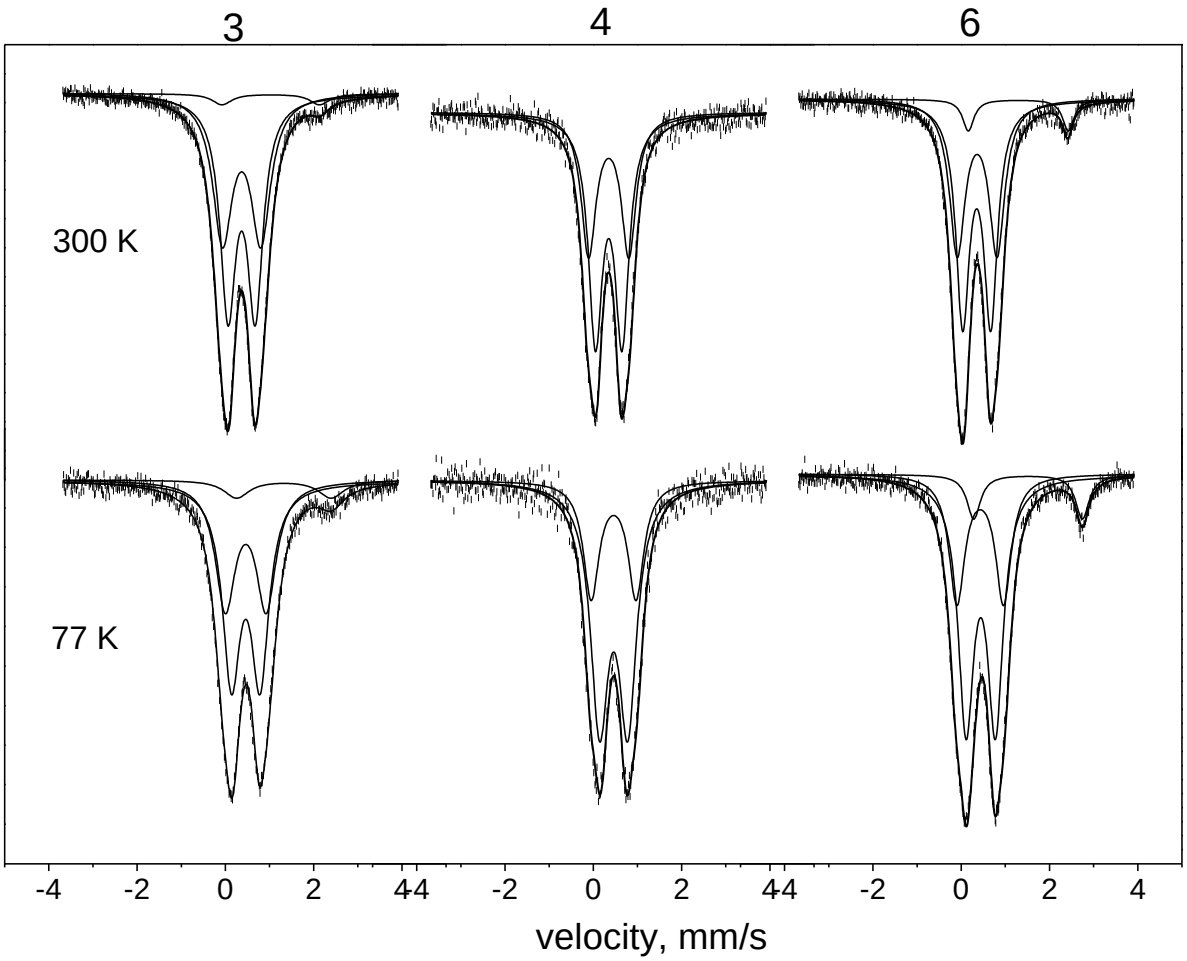

Fig. 6. The Mössbauer spectrum of **3**, **4** and **6** at 300 and 77K.

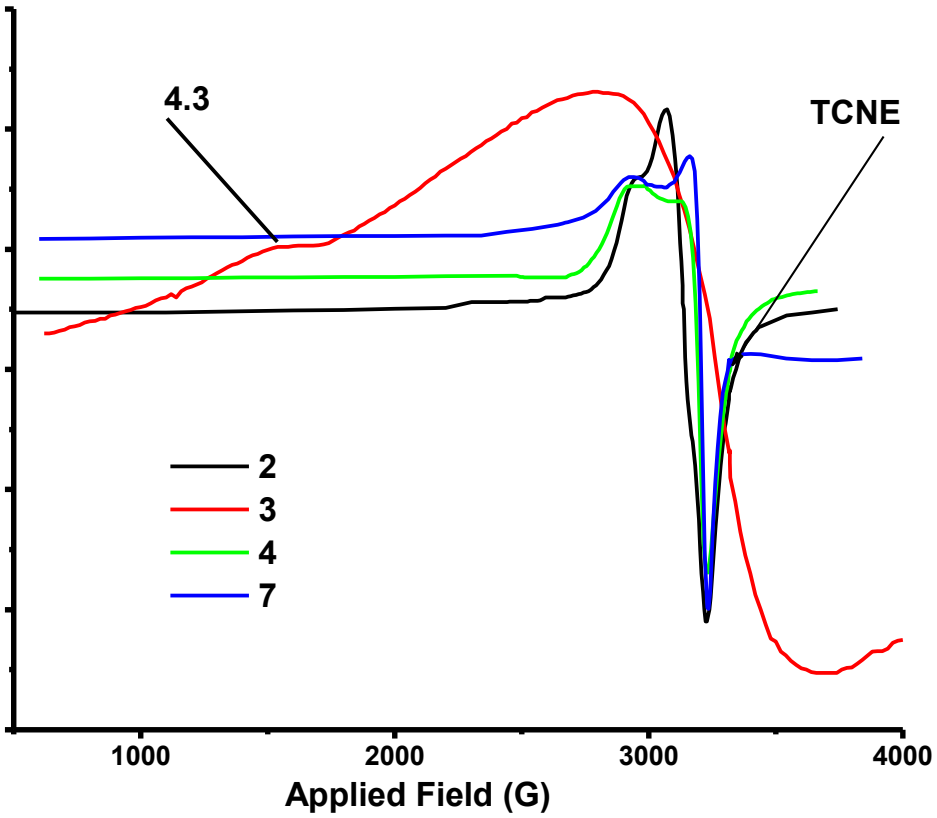

Fig. 7. Solid state EPR spectra of **2**, **3**, **4** and **7** at RT.

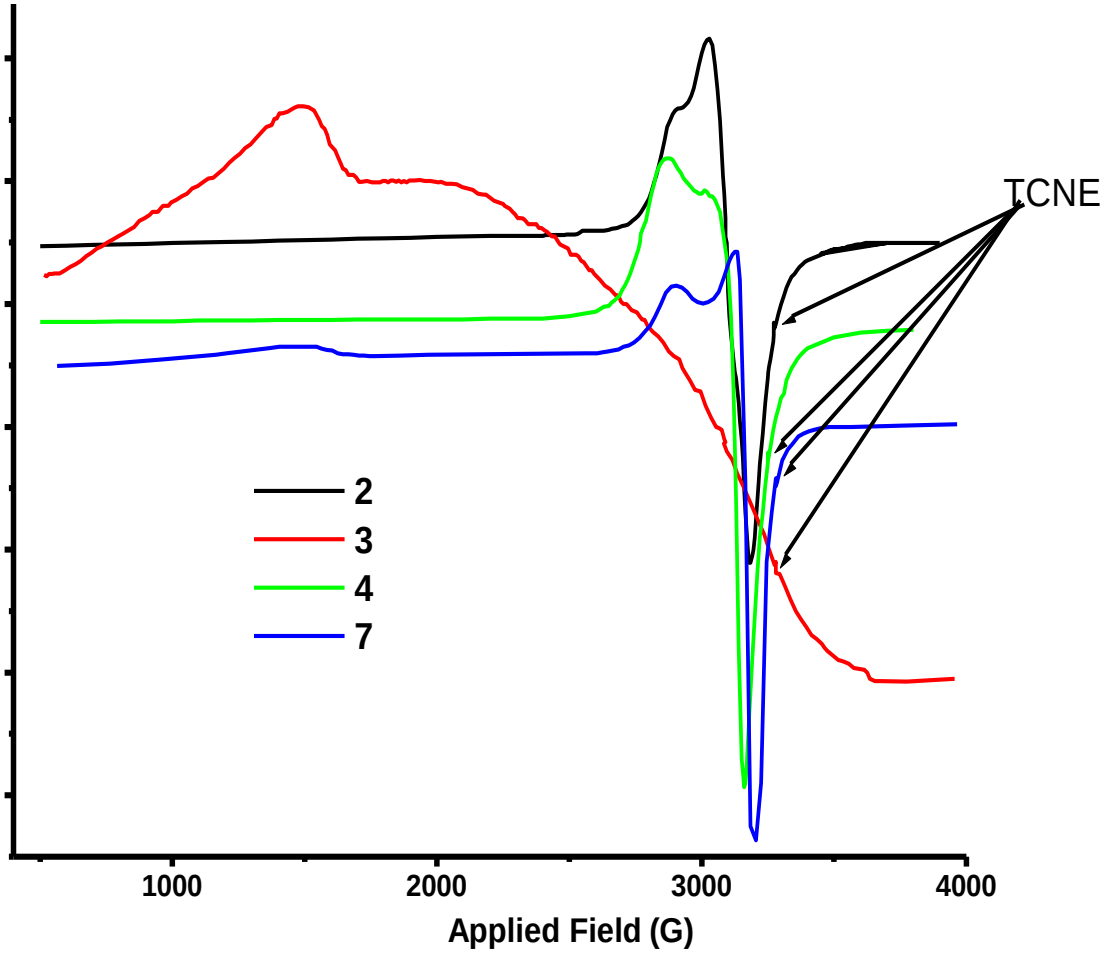

Fig. 8. Solid state EPR spectra of **2**, **3**, **4** and **7** at LNT.

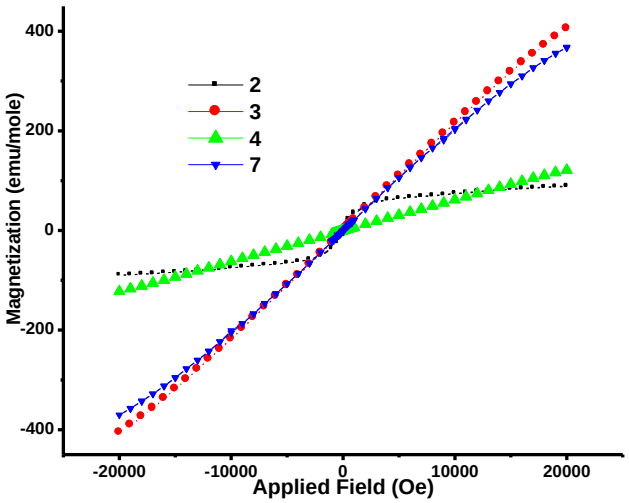

Fig. 9(a) M-H curve of polymers **2**, **3**, **4** and **7**.

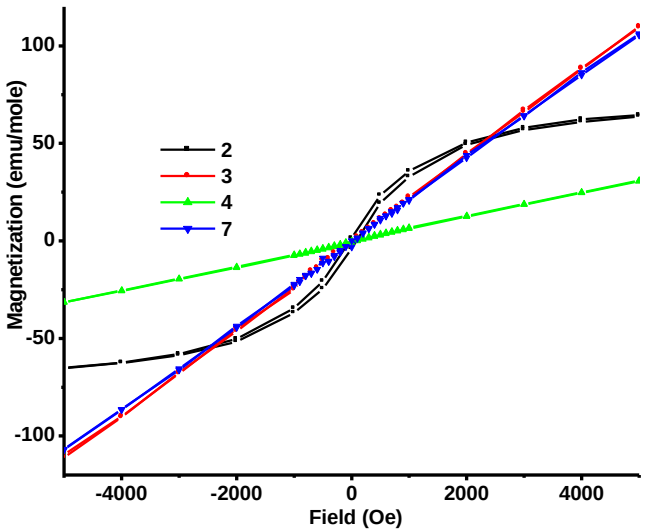

Fig. 9(b). M- H under low field region.

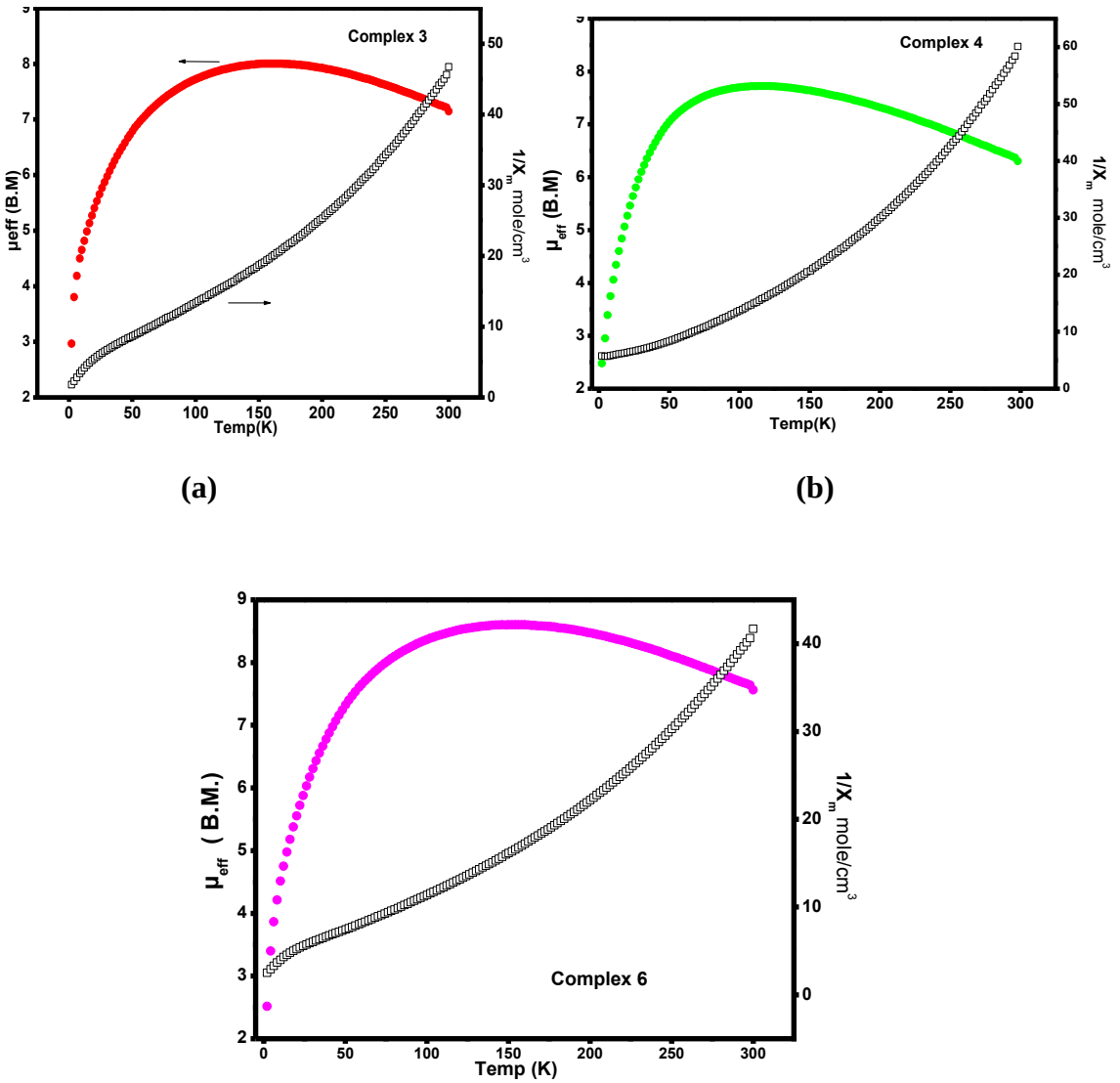

Fig. 10 (a-c). Temperature dependence of μ_{eff} and χ_m^{-1} **(a)** for **3**, **(b) 4** and **(c) 6.**

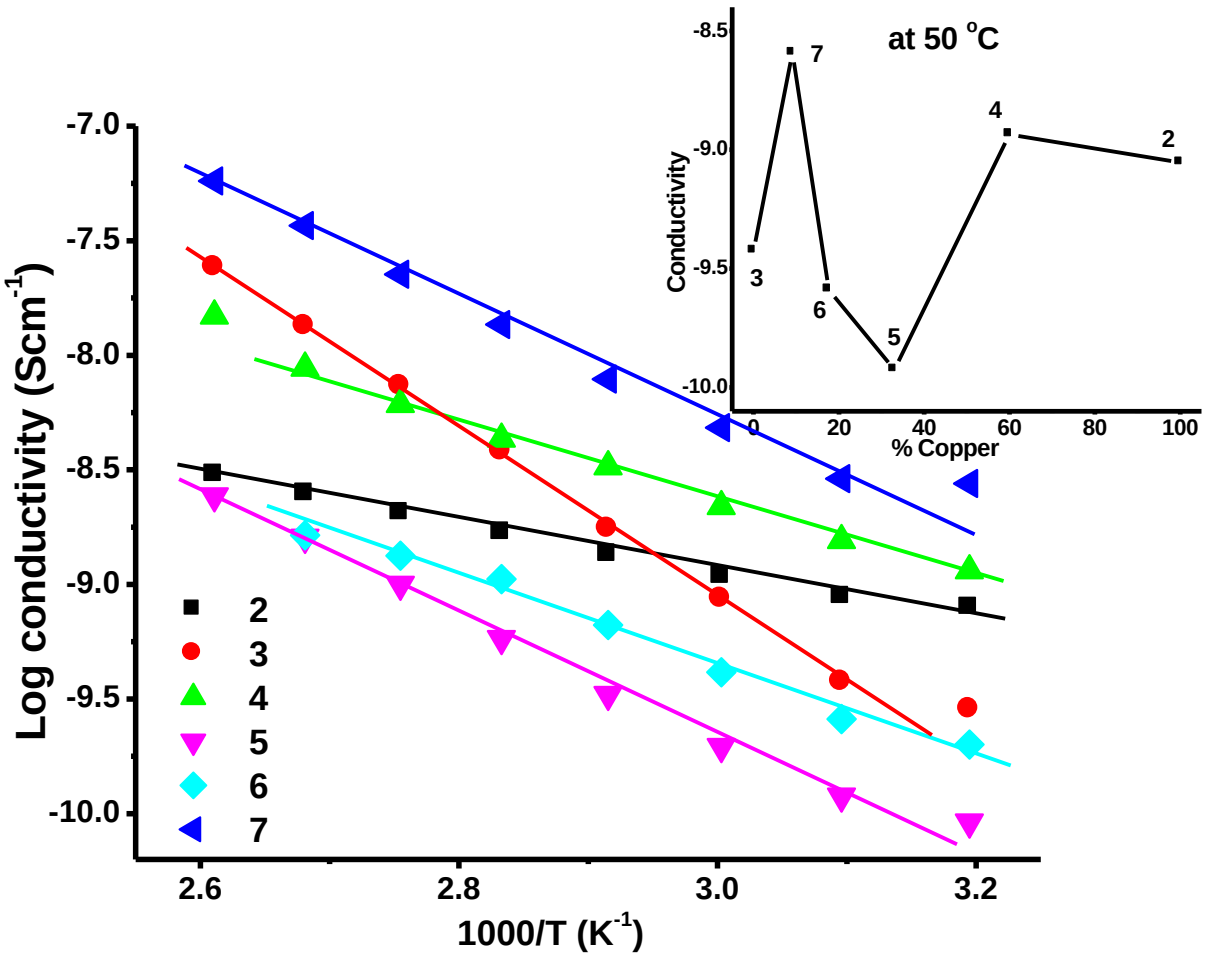

Fig. 11. Variable temperature solid state electrical conductivity of the polymers **2**-**7**. The inset image shows variation of conductivity as a function of dopant concentration at 50°C.